doi:10.1093/brain/awu155 Brain 2014: 137; 2312–2328 | 2312

BRAIN
A JOURNAL OF NEUROLOGY

Temporal dynamics of hippocampal neurogenesis in chronic neurodegeneration

Diego Gomez-Nicola,[1] Stefano Suzzi,[1] Mariana Vargas-Caballero,[1,2] Nina L. Fransen,[1] Hussain Al-Malki,[1,3] Arantxa Cebrian-Silla,[4] Jose Manuel Garcia-Verdugo,[4] Kristoffer Riecken,[5] Boris Fehse[5] and V. Hugh Perry[1]

1 Centre for Biological Sciences, University of Southampton, Southampton, UK
2 Institute for Life Sciences, University of Southampton, Southampton, UK
3 University College in Al-Qunfudah, Umm Al-Qura University, Saudi Arabia
4 Laboratory of Comparative Neurobiology, Instituto Cavanilles de Biodiversidad y Biologia Evolutiva, University of Valencia, CIBERNED, Valencia, Spain
5 Research Department Cell and Gene Therapy, Clinic for Stem Cell Transplantation, University Medical Centre (UMC) Hamburg-Eppendorf, Hamburg, Germany

Correspondence to: Diego Gomez-Nicola PhD,
Centre for Biological Sciences, University of Southampton,
South Lab and Path Block,
Mail Point 840, LD80C,
Southampton General Hospital,
Tremona Road, SO16 6YD,
Southampton, UK
E-mail: d.gomez-nicola@soton.ac.uk

The study of neurogenesis during chronic neurodegeneration is crucial in order to understand the intrinsic repair mechanisms of the brain, and key to designing therapeutic strategies. In this study, using an experimental model of progressive chronic neurodegeneration, murine prion disease, we define the temporal dynamics of the generation, maturation and integration of new neurons in the hippocampal dentate gyrus, using dual pulse-chase, multicolour γ-retroviral tracing, transmission electron microscopy and patch-clamp. We found increased neurogenesis during the progression of prion disease, which partially counteracts the effects of chronic neurodegeneration, as evidenced by blocking neurogenesis with cytosine arabinoside, and helps to preserve the hippocampal function. Evidence obtained from human post-mortem samples, of both variant Creutzfeldt-Jakob disease and Alzheimer's disease patients, also suggests increased neurogenic activity. These results open a new avenue into the exploration of the effects and regulation of neurogenesis during chronic neurodegeneration, and offer a new model to reproduce the changes observed in human neurodegenerative diseases.

Keywords: neural stem cells; adult neurogenesis; Alzheimer's disease; variant CJD

Abbreviations: BrdU = 5-bromo-2'-deoxyuridine; CJD = Creutzfeldt-Jakob's disease; EdU = 5-ethynyl-2'-deoxyuridine; PrP = prion protein

Introduction

Adult neurogenesis permits the regeneration of certain neuronal populations in the CNS. In mammals, neural stem cells are mainly located within the subventricular zone and the subgranular zone of the dentate gyrus, giving rise to olfactory bulb neurons and hippocampal granule cells, respectively (Alvarez-Buylla *et al.*, 2002). The neurogenic capability of the adult brain is tightly

Received February 4, 2014. Revised April 23, 2014. Accepted April 25, 2014. Advance Access publication June 18, 2014

regulated after brain injury. Several studies indicate that neurogenesis is increased during acute or chronic neurodegeneration, with the potential to replace damaged neurons at the lesion sites (Winner *et al.*, 2011). In response to diverse experimental lesions, including stroke, ischaemia or epilepsy, precursor cells proliferate and migrate to the sites of damage (Arvidsson *et al.*, 2002; Parent *et al.*, 2002). Studies in models of Alzheimer's disease that capture the amyloid deposition and limited studies in human post-mortem tissue suggest an influence of the disease on the hippocampal neurogenic response, although contradictory views exist (Marlatt and Lucassen, 2010). Analysis of post-mortem human Alzheimer's disease hippocampi showed increased cell proliferation, associated with increased neurogenesis (Jin *et al.*, 2004) or alternatively with increased gliosis and vascular changes (Boekhoorn *et al.*, 2006). The use of transgenic models of Alzheimer's disease has shed some light on the regulation of neurogenesis, although a similar controversy of that of human Alzheimer's disease is still present in the literature (for review see Winner *et al.*, 2011). Differences among models, experimental conditions and age of examined subjects may account for the discrepancies arising from animal studies, together with the fact that none of the transgenic models established so far display extensive loss of hippocampal neurons and, if any, are mainly restricted to the CA1 layer leaving the dentate gyrus spared (Schmitz *et al.*, 2004; Rupp *et al.*, 2011). These mixed findings highlight the need for a better understanding of the neurogenic response triggered by chronic progressive neurodegeneration in the adult.

Prion diseases are a group of fatal, chronic progressive and transmissible neurodegenerative diseases, characterized by progressive vacuolation, neuronal cell loss and gliosis (Masters and Richardson, 1978; Williams *et al.*, 1997). Prion disease experimental models are tractable laboratory models to study protein misfolding and neuronal degeneration, common to several neurodegenerative diseases. Although some features of prion disease such as the gliotic response or the neurodegenerative process have been extensively characterized, the role of neurogenesis in prion disease has not been addressed in detail yet. Cellular prion protein (PrP^c, now known as PRNP) has been shown to be expressed in non-mitotic cells at the subventricular zone and to control normal neural stem cell differentiation to a neuronal phenotype. The transgenic overexpression of PrP^c is associated with an increased proliferation in the subventricular zone. However, PrP^c expression levels do not affect the final neuron number in the dentate gyrus (Steele *et al.*, 2006). Studies with doppel (now known as PRND), a protein with biochemical and structural homology with PrP^c, showed normal neural differentiation of stem cells when its gene was mutated (Behrens *et al.*, 2001). More interestingly, recent work supports the hypothesis that the generation of PrPSc (misfolded form of PrP^c) in cultured neural stem cells impairs neuronal differentiation (Relano-Gines *et al.*, 2013). There is thus a need for a detailed analysis of the dynamics, regulation and functional implications of the neurogenic response during prion disease, in order to better understand this complex pathology.

In this study we investigated the dynamics and regulation of neurogenesis during the temporal course of chronic neurodegeneration, rather than simply studying a terminal time-point that would not be informative of the responses taking place in the brain during disease evolution and progression. Experimental models of prion disease are robust and reproducible models of neurodegeneration, with a well-documented temporal and spatial sequence of steps of gliosis, inflammation, synaptopathy and neurodegeneration; aspects that make them ideal for the study of a dynamic system like neurogenesis and that cannot be readily obtained by using alternative transgenic or experimental models of neurodegeneration (Perry, 2010). We studied neurogenesis in a prion disease model as this would provide a basis for manipulating neurogenesis and evaluating its impact on both behaviour and pathology.

Materials and methods

Experimental models of prion disease

Female C57BL/6J mice (Harlan) were bred and maintained in local facilities. Mice were housed in groups of 4 to 10, under a 12-h light/12-h dark cycle at 21°C, with food and water *ad libitum*. To induce prion disease, mice were anaesthetized with a ketamine/rompun mixture (85 and 13 mg/kg), and 1 µl of either ME7-derived (ME7 animals) or 22L-derived (22L animals) brain homogenate (10% w/v) or normal brain homogenate (NBH animals) was injected stereotaxically and bilaterally at the CA1 layer of the dorsal hippocampus, at coordinates from bregma: anteroposterior, −2.0 mm; lateral, ±1.7 mm; depth, 1.6 mm. All procedures were performed in accordance with UK Home Office licensing.

Clinical samples of variant Creutzfeldt-Jakob's disease and Alzheimer's disease

Human brain autopsy tissue samples (paraffin-embedded, formalin-fixed, 96% formic acid-treated, 6 µm sections) from the National CJD Surveillance Unit Brain Bank (Edinburgh, UK) were obtained from cases of variant Creutzfeldt-Jakob's disease (variant CJD; five females and five males, age 20–34 years), Alzheimer's disease (five females and five males, age 58–76 years) or the correspondent age-matched controls (variant CJD controls: five females and five males, age 20–35 years; Alzheimer's disease controls: four females and five males, age 58–79 years), of whom consent for use of autopsy tissues for research had been obtained. All cases fulfilled the criteria for the pathological diagnosis of variant CJD or Alzheimer's disease. None of the cases had any of the known mutations of the *PRPN* gene or family history of prion disease, and there was no evidence of the common types of iatrogenic aetiology. Ethical permission for research on autopsy materials stored in the National CJD Surveillance Unit was obtained from Lothian Region Ethics Committee.

5-Ethynyl-2′-deoxyuridine and 5-bromo-2′-deoxyuridine dual labelling

The study of proliferation and differentiation of neural stem cells in the dentate gyrus was performed by sequential incorporation of 5-ethynyl-2′-deoxyuridine (EdU) or 5-bromo-2′-deoxyuridine (BrdU) (Gomez-Nicola *et al.*, 2011), to allow the analysis of proliferation and differentiation in the same experimental samples, minimizing the use of animals (Supplementary Fig. 4). EdU (Click-iT EdU Imaging Kit;

Invitrogen) was used to study cell differentiation, and administered at 8 or 12 weeks post-induction of the NBH or ME7 groups (intraperitoneal 7.5 mg/ml in PBS, 0.1 ml/10 g mouse). The animals were injected with BrdU at 8 (without prior injection of EdU), 12 (injected with EdU at 8 weeks) or 20 (injected with EdU at 12 weeks post-induction) weeks post-induction of the NBH or ME7 groups (intraperitoneal 7.5 mg/ml in PBS, 0.1 ml/10g mouse) and perfused 24 h later. BrdU was visualized as described in the immunohistochemistry section and EdU was visualized using the Click-iT reaction coupled to an Alexa Fluor® 568 azide following the instructions of the manufacturer (Invitrogen).

Ablation of neurogenesis by cytosine arabinoside

ME7 (prion) mice were treated with 2% cytosine arabinoside (Sigma-Aldrich; $n = 4$), a dose previously used and extensively reported to have no detrimental effects on non-dividing cells (Doetsch *et al.*, 1999). We used sterile saline (vehicle; $n = 4$) as vehicle, and treatments were performed for 1 month (from Week 12 to 16 post-infection), using an intraventricular brain infusion kit (Alzet; anteroposterior, 0.0 mm; lateral, −1.0 mm) coupled to an osmotic mini-pump (Alzet; model 1004, flow 0.11 µl/h). Mice received two daily intraperitoneal injections of BrdU (Sigma-Aldrich; 7.5 mg/ml, 0.1 ml/10 g weight in sterile saline), before the end of the experiment (16th week). The pump's weight was measured before and after the experiment, and the placement of the intraventricular cannula was checked to ensure correct delivery of the treatments in each animal.

Cloning of viral vectors and generation of viral particles

Design, production and application of γ-retroviral vectors to the study of adult neurogenesis will be described in detail elsewhere (unpublished data), and derives from the previously described lentiviral gene-ontology vectors (LeGO) (Weber *et al.*, 2008), used for the RGB marking technique (Weber *et al.*, 2011, 2012). Briefly, the viral vectors used in this study were derived from the γ-retroviral vector RSF91.GFP.pre* (Schambach *et al.*, 2006*b*), whose marker gene (enhanced green fluorescent protein, eGFP) has been replaced by the two fluorescent proteins Venus and mCherry, respectively. mCherry was amplified from LeGO-C2 (Weber *et al.*, 2008) by PCR (Fw-Primer: 5′-ATATACCGGTCGCCACCATGGTGAGCAAGG; Rv-Primer: 5′-CGAAGTTATTAGGTCCCTCGACG) and cloned into RSF91.GFP.pre* using AgeI and BsrGI. Venus has been cut out from LeGO-V2 (Weber *et al.*, 2008) and cloned into RSF91.GFP.pre* using NcoI and BsrGI. Standard procedures of molecular cloning were used to generate all viral vectors. The sequence of every DNA fragment cloned by PCR has been verified by sequencing. The two retroviral vectors express their fluorescent protein under the control of an enhancer/promoter cloned from the spleen focus-forming virus (Baum *et al.*, 1997) (SFFV promoter) within the long terminal repeats (LTR). Vector maps and sequence data for all vectors are available upon request; more information can be found at http://www.LentiGO-Vectors.de.

Cell-free supernatants containing viral particles were produced by transient transfection of HEK-293T packaging cells as described (Schambach *et al.*, 2006*b*; Weber *et al.*, 2012). γ-Retroviral vectors were packaged using pcDNA3.MLVgp (Schambach *et al.*, 2006*a*) and K73-Eco expressing the envelope protein of ecotropic murine leukaemia virus (Morita *et al.*, 2000). Supernatants containing γ-retroviral particles were concentrated ∼100-fold by centrifugation at 8000*g* and 6°C for 8 to 12 h. Concentrated supernatants were titrated (Weber *et al.*, 2012) on NIH-3T3 cells, suitable for Eco pseudotypes. For titration, target cells were incubated at 5×10^4 cells in 0.5 ml medium in each well of a 24-well plate in the presence of 8 µg/ml polybrene. After addition of particle-containing supernatant, the plate was centrifuged at 1000*g* for 1 h at 25°C. Initial gene transfer rates were analysed 48 to 72 h after transduction by fluorescence-activated cell sorting (FACS). The following cytometers were used to acquire FACS data (Becton Dickinson): FACSCantoII (405/488/635 nm lasers) and LSRFortessa (405/488/561/640 nm lasers). Titres of $\sim 1.5 \times 10^9$ virus particles per ml concentrated supernatant were obtained for the two vector types (range: $0.9–2.6 \times 10^9$/ml).

Tracing of hippocampal neurogenesis with γ-retroviral vectors

The sequential delivery of Venus or mCherry vectors was used to trace three windows of hippocampal neurogenesis in NBH or ME7 mice. Mice were anaesthetized with a ketamine/rompun mixture (85 and 13 mg/kg), and 1 µl (10^9 particles/ml) of the viral particles were injected stereotaxically and bilaterally at each of the following coordinates from bregma: dentate gyrus (hilus), anteroposterior, −2.0 mm; lateral, ±1.3 mm; depth, −2 mm and anteroposterior, −1.5 mm; lateral, ±0.8 mm; depth, −2 mm.

Mouse perfusion, tissue processing and analysis were performed as previously described (Gomez-Nicola *et al.*, 2011). Coronal sections were cut with a vibrating microtome from paraformaldehyde-fixed brains (50 µm). After repeated rinses with PBS, and counterstaining with DAPI (Sigma-Aldrich), free-floating sections were mounted onto glass slides and coversliped with a Mowiol®/DABCO (Sigma-Aldrich) mixture. Sections were visualized on a Leica TCS-SP5 confocal system, coupled to a Leica CTR6500 microscope. Confocal stacks were acquired using 1-µm *z*-steps to cover the whole morphology of the labelled cells and their processes. Cells within the dorsal and ventral blade of the dorsal dentate gyrus were analysed in this study.

Sholl analysis was performed on 3D reconstructions of confocal *z*-stacks to analyse the dendritic-tree complexity (Sholl, 1953). Briefly, the number of crossings for concentric circles of given radii centred at the tree stem (Sholl number) was calculated. Starting radius and radius step size were set each at 10 µm up to 300 µm. A total of 120 neurons were analysed, of which 51 were from NBH animals and 69 were from ME7 animals.

For the dendritic linear spine density, confocal stacks of γ-retrovirally-labelled apical dendritic processes of dentate granule cells extending through the molecular layer were acquired, generating maximum intensity projections along the *z*-axis. Dendritic linear spine density was calculated by dividing the total number of spines on a given dendrite by the length of that dendrite. A total of 165 dendrites were analysed, of which 94 were from NBH animals and 71 were from ME7 animals.

Confocal stacks of γ-retrovirally-labelled mossy fibre axon terminals in the stratum lucidum were acquired, generating maximum intensity projections along the *z*-axis. Mossy fibre boutons were selected for measurement by following criteria established previously (Toni *et al.*, 2008). Bouton size was evaluated by manually tracing each bouton and then measuring the enclosed area, quantifying the average size for each group. A total of 405 boutons were analysed, of which 219 were from NBH animals and 186 were from ME7 animals.

All quantifications were performed with the help of the ImageJ image analysis software, additionally using NeuronJ and Sholl Analysis plug-ins.

Patch-clamp recordings of granule cells

A group of mice were injected with γ-retroviral Venus-expressing vectors, as previously described, 14 weeks post-induction of prion disease (ME7) using NBH as controls. Four weeks later, mice were anaesthetized with pentobarbital and perfused with oxygenated (95% O_2, 5% CO_2) ice-cold artificial CSF through the heart. The artificial CSF contained (in mM): 126 NaCl, 3 KCl, 1.25 NaH_2PO_4, 2 $MgSO_4$, 2 $CaCl_2$, 26 $NaHCO_3$, and 10 glucose, pH 7.3–7.4. The brain was dissected out and placed in ice-cold artificial CSF. For brain slice preparation and storage, a low-sodium oxygenated solution containing (in mM) 64 NaCl, 120 sucrose, 25 $NaHCO_3$, 10 glucose, 2.5 KCl, 1.25 NaH_2PO_4, 0.5 $CaCl_2$ and 7 $MgCl_2$ was used. Coronal brain slices (350 μm) were prepared using a vibrating microtome (Camden Instruments).

After recovering at room temperature (22–25°C) for at least 1 h, slices were transferred to the recording chamber and superfused with oxygenated artificial CSF at a rate of 1–2 ml/min. Recordings were performed under visual control. Patch pipettes (4–6 MΩ) were pulled from thick-walled borosilicate glass tubing and filled with a solution containing (in mM): 110 potassium-gluconate, 40 HEPES, 2 ATP-Mg, 0.3 GTP, 4 NaCl (pH 7.25 adjusted with KOH; osmolarity 280–290 mosmol/l). Slices were viewed with an upright microscope (Axioskop, Zeiss), and whole-cell patch clamp recordings were obtained using infrared, differential interference contrast optics combined with epifluorescence to visualize either green fluorescent (Venus+) and non-fluorescent cells in the granule layer of the dentate gyrus. Recordings were carried out at room temperature using an amplifier Axopatch 200B (correction knob at 100% to enable bridge balance) or a Multiclamp 700B (Molecular Devices) (current clamp in bridge-mode). The holding potential was set to −75 mV by injecting <30 pA. Current pulses of 300-ms duration of increasing amplitude from −200 pA to 800 pA were used to test excitability in current clamp. Input resistance was measured in voltage clamp with 50 ms 2 mV pulses. Signals were low-pass filtered at 5 kHz and sampled at 20 kHz with 16-bit resolution, using a National Instruments analogue card, and custom software written in Matlab and C (MatDAQ, Hugh Robinson, 1995–2013). All analysis was performed in Matlab (Mathworks).

Biotinylated dextran amine tracing

Retrograde tracing of the mossy fibre pathway was performed by stereotactic injection of biotinylated dextran amine in the CA3 region of the hippocampus. At 16 weeks post-induction NBH or ME7 mice ($n = 4$) were injected stereotaxically and bilaterally with 0.1 μl of biotinylated dextran amine (10 000 MW, Molecular probes; 10% w/v in sterile H_2O) in the CA3 region of the hippocampus at the coordinates from bregma: anteroposterior, −1.7 mm, 2.2 mm lateral, 1.5 mm depth. The surgery was carried out as described above (induction of experimental prion disease), using a glass micropipette to inject biotinylated dextran amine, with an outer diameter of ~15–20 μm, recommended to significantly reduce the damage to neurons and diffusion of the tracer at the injection sites. The survival time after injection of the tracer was first optimized in naive mice, and set to 2 days after the injection of the tracer to achieve optimal labelling of the mossy fibre pathway.

The visualization of the biotinylated dextran amine was performed as previously described (Veenman *et al.*, 1992). Briefly, the sections were first incubated in 3% H_2O_2 (Sigma-Aldrich) for 30 min to block the endogenous peroxidase activity, followed by amplification with the Vectastain ABC Kit (Vector) in 0.3% PBS with Triton™ X-100. Phosphate buffer (0.1 M) was used to wash after every step of the protocol. Biotinylated dextran amine was visualized using diaminobenzidine precipitation, in a Leica CTR 5000 microscope, coupled to a Leica DFC300FX microscope camera.

Golgi-Cox staining

A subgroup of ME7 animals ($n = 3$; 18 weeks post-induction) were deeply anaesthetized with sodium pentobarbital and then transcardially perfused with artificial CSF. Brains were then rapidly dissected and sliced with a vibrating microtome (200 μm; Leica). The hippocampal slices were incubated in rapid Golgi-Cox solutions, following manufacturer's instructions (FD Rapid GolgiStain™ Kit, FD Neurotechnologies). The slices were infused with a solution containing potassium dichromate, potassium chromate and mercuric chloride for 2 weeks, to be further developed into the Golgi-Cox staining on free-floating plates. The slices were mounted onto gelatinized slides, dried, dehydrated, cleared with xylene and mounted with DPX. Golgi-treated slices were analysed with a Leica CTR 5000 microscope, coupled to a Leica DFC300FX microscope camera.

Ultrastructural characterization of newborn granule cells

For pre-embedding immunogold staining, mice were perfused with 4% paraformaldehyde/0.5% glutaraldehyde, post-fixed in 4% paraformaldehyde, and 50-μm sections were cut on a vibratome (Leica). Pre-embedding immunogold staining was performed by incubating sections in chicken anti-GFP primary antibody (1:200, Aves Lab) and in the appropriate colloidal gold-conjugated secondary antibody (1:50; UltraSmall; Aurion). The samples were post-fixed in 1% osmium and 7% glucose for 30 min, rinsed, dehydrated, and embedded in araldite (Durcupan; Fluka). For the ultrastructural characterization of Venus-positive dendrites, serial ultrathin sections (60–70 nm) were cut with a diamond knife, stained with lead citrate, and examined under a transmission electron microscope (Tecnai Spirit G2; FEI) and images recorded using a digital camera (Morada, Soft Imaging System; Olympus). Adjustment of brightness and contrast of the pictures, if needed, was performed with Adobe Photoshop (Adobe Systems).

Immunohistochemistry

Coronal hippocampal sections were cut from paraformaldehyde-fixed, frozen or fresh brains, or wax-embedded tissue. Mice perfusion, tissue processing and immunohistochemical analysis was performed as previously described (Gomez-Nicola *et al.*, 2008, 2014) using the following primary antibodies: rabbit anti-PCNA (Abcam), rabbit anti-phospho-Histone H3 (Cell Signaling), rabbit anti-Ki67 (Abcam), mouse anti-BrdU (DSHB), rat anti-BrdU (Santa Cruz Biotechnologies), goat anti-doublecortin (DCX; Santa Cruz Biotechnologies), guinea pig anti-doublecortin (DCX; Millipore), rabbit anti-calretinin (Millipore), goat anti-Sox2 (Santa Cruz Biotechnologies), mouse anti-NeuN (Millipore), mouse anti-synaptophysin (Millipore) and rabbit anti-cleaved caspase 3 (Millipore). After primary antibody incubation, the sections were washed and incubated with the appropriate biotinylated secondary antibody (Vector Labs), and/or with the appropriate Alexa Fluor® 405, 488 or 568 conjugated secondary antibody or streptavidin

(Molecular Probes). The blocking, primary antibody and secondary antibody incubations were performed using PBS + Tween20 (0.2%) as diluent. A minimum of three washes with PBS + Tween20 (0.2%) was completed between steps. For light microscopy, the sections were visualized after diaminobenzidine precipitation, in a Leica CTR 5000 microscope, coupled to a Leica DFC300FX microscope camera. When required, the diaminobenzidine signal was enhanced with 0.05% nickel ammonium sulphate, producing a black precipitate. After immunofluorescence labelling, nuclei were visualized by DAPI or Hoechst staining and the sections were mounted with Mowiol®/DABCO (Sigma-Aldrich) mixture. The sections were visualized on a Leica TCS-SP5 confocal system, coupled to a Leica CTR6500 microscope.

The general immunohistochemistry protocol was modified for the detection of BrdU, adding a DNA denaturation step with 2 N HCl (30 min, 37°C), as previously described (Gomez-Nicola *et al.*, 2011, 2013).

The protocol used for immunohistochemistry on human sections was a modification of the general protocol, with antigen unveiling in boiling citrate buffer (pH 6.0) being performed for 25 min.

Quantification and image analysis

The quantification of antigen positive cells was performed in dentate gyrus (DCX, Calretinin, NeuN, Caspase 3) or subgranular layer (pHH3, PCNA, BrdU, Sox2) ($n = 4$ fields/mouse, $n = 4$–8 mice/group) after diaminobenzidine immunohistochemistry. The quantification of the intensity of signal (i.e. synaptophysin) was performed after diaminobenzidine immunohistochemistry or immunofluorescence, and presented as per cent stained area (grey value stratum lucidum versus granular layer). The number of double positive cells (i.e. EdU + NeuN +) in the specific area ($n = 4$ fields/mouse, $n = 4$–8 mice/group) was performed after double immunofluorescence. Data were represented as number of positive cells/mm^2. Measurements of the mouse dentate gyrus thickness were obtained by sampling five symmetric points of the ventral and dorsal blades of the dentate gyrus at the dorsal hippocampal level ($n = 4$–8 mice/group). The quantification of antigen positive cells (i.e. Ki67 +) in human brains was performed in the hippocampal dentate gyrus after diaminobenzidine immunohistochemistry ($n = 9$–10 brains/group; 4–5 $\times 20$ fields/sample). All quantifications were performed with the help of the ImageJ image analysis software.

Statistical analysis

Data were expressed as mean ± standard error of the mean (SEM) and analysed with the GraphPad Prism 5 software package (GraphPad Software). For all data sets, normality and homoscedasticity assumptions were reached, validating the application of the one-way or two-way ANOVA, followed by the Tukey *post hoc* test for multiple comparisons. *T*-test was used when the comparison of only two experimental groups was necessary. Differences were considered significant for $P < 0.05$.

Results

Temporal dynamics of hippocampal neurogenesis during prion disease

We studied the proliferative activity in the subgranular layer of the dentate gyrus in the ME7 model of prion disease. We observed a statistically significant increase in the number of proliferative cells in the subgranular layer, detected as PCNA + or phospho-histone H3 (pHH3) + cells (Fig. 1A and B), when compared with the NBH (normal brain homogenate) controls. These results correlate with an observed increase in the number of cells incorporating BrdU (short-term pulse) within the subgranular layer, which increase as the disease progresses (Fig. 1C and D). A large number of proliferating cells were found outside the subgranular layer of the dentate gyrus, identified as BrdU + EGFP-c-fms + microglia (Supplementary Fig. 1), correlating with previously reported data (Gomez-Nicola *et al.*, 2013). This progressive increase in proliferation in the subgranular layer in prion disease does not correlate with the temporal course of generation of neural progenitor cells, detected as doublecortin- (DCX) or calretinin-positive cells within the subgranular layer (Fig. 1E and F). We observed an initial significant increase in the number of neural progenitors during early and mid-stages of prion disease that returns to levels comparable with NBH animals at the end of the disease (Fig. 1E and F). The results in the ME7 model of prion disease were similar to those found in the 22L model (Supplementary Table 1), with a significant increase in the number of proliferating cells (PCNA + and pHH3 +) and neural precursor cells (DCX +) in the subgranular layer. The population of neural stem cells (Sox2 +) did not show any significant change in numbers (Fig. 1F), whereas the number of BrdU + /DCX + intermediate precursor cells increased (Fig. 1G), thus suggesting that the amplification of the neurogenic pool was generated later on in the differentiation pathway. Our results also indicate the occurrence of 'hot-spots' of neurogenesis in prion disease, as both the markers of proliferation and neurogenesis were condensed in small clusters at the subgranular layer (Fig. 1B, D, E and G).

These results show that there is increased generation of dentate gyrus neural precursors during the progression of prion disease, potentially providing an active replacement of neurons to balance the ongoing neurodegeneration.

The increased neurogenesis during prion disease is effective in maintaining the integrity of the dentate gyrus during neurodegeneration

We next investigated whether the observed increase in neurogenesis during prion disease is associated with the full differentiation into neurons (Fig. 2). As prion disease evolves, progressive neurodegeneration occurs in the hippocampus, with loss of neurons in the CA1 and CA3 layers (Fig. 2A). In contrast, the cellular integrity of the dentate gyrus is preserved during the disease (Fig. 2A and B), indicating either minimal neurodegeneration or a self-repairing mechanism being in place. The first possibility was ruled out as we observed a high and maintained rate of neuronal apoptosis (cleaved caspase 3 expression) in the dentate gyrus, from early stages of the disease, contrasting with the later progressive increase in the number of apoptotic cells observed in both CA1 and CA3 (Fig. 2C–E). The early apoptotic response in the dentate gyrus correlates with the pattern of deposition of PrPSc, preferentially locating in the dentate gyrus from early stages of the disease (Supplementary Fig. 2). The preservation of the dentate gyrus

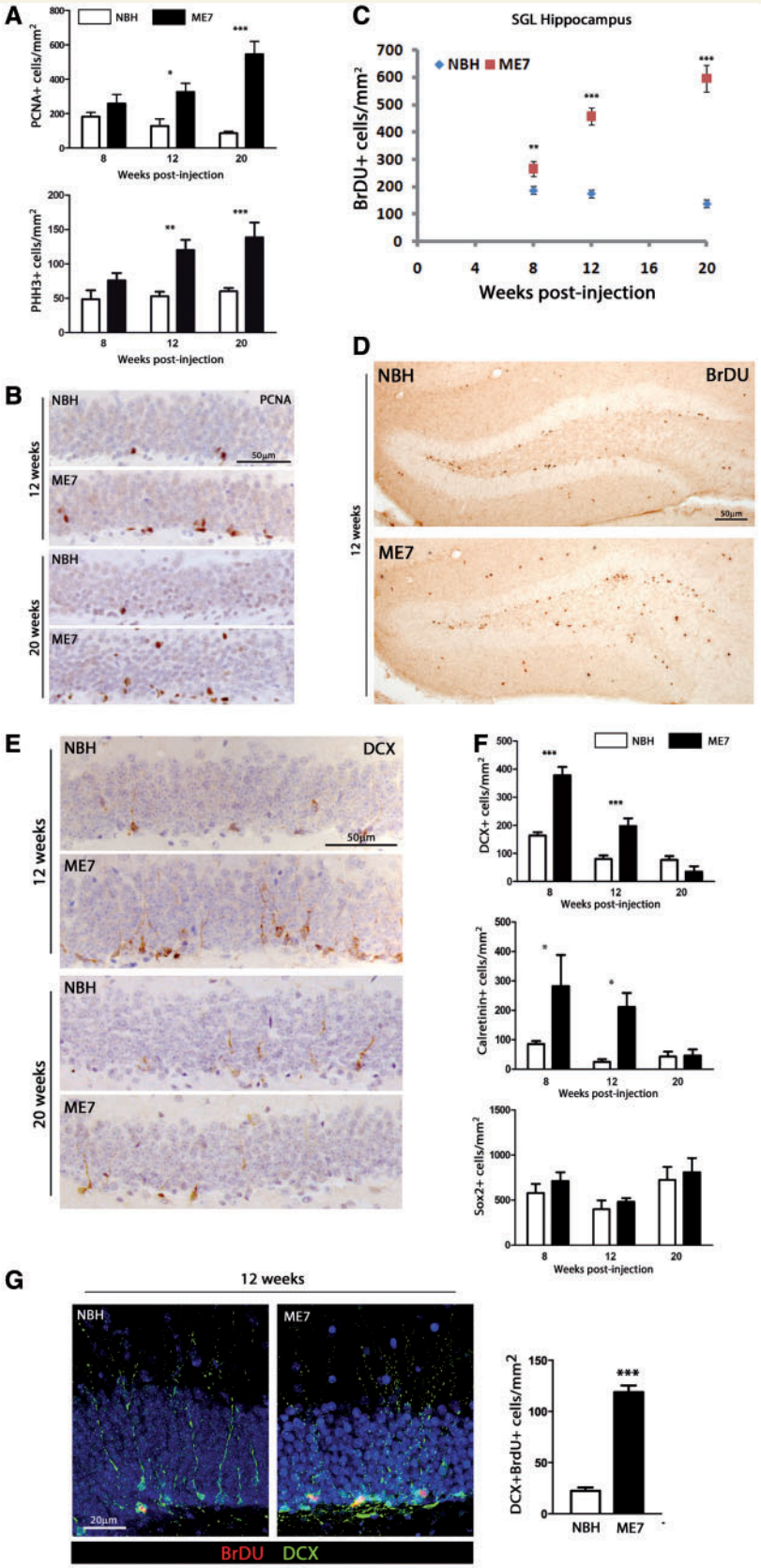

Figure 1 Temporal analysis of hippocampal neurogenesis in prion disease. (**A** and **B**) Immunohistochemical analysis of the temporal expression of the markers of proliferation PCNA and phospho-histone H3 (pHH3) at the subgranular layer (SGL) of the dentate gyrus of prion disease (ME7; black bars) and control (NBH; open bars) mice (see representative images for PCNA, **B**). Quantified data expressed as mean ± SEM of the number of PCNA+ or pHH3+ cells/mm^2. (**C** and **D**) Immunohistochemical analysis of the incorporation of BrdU

(continued)

integrity was also found in the 22L mice, evidence of a cellular response comparable to that observed in the ME7 model (Supplementary Table 1). With the preservation of the dentate gyrus being the net result, we evaluated the efficacy of the observed increased neurogenic response to compensate for the increased neurodegeneration in pulse-chase experiments (Fig. 2F and G). We administered EdU (8 weeks), and detected it in mature granule cells (NeuN+) of the dentate gyrus at 12 or 20 weeks post-induction, demonstrating an increased and significant neuronal replacement rate, when compared with that of the NBH controls (Fig. 2F and G).

To understand the contribution of the increased neurogenic activity to the preservation of the dentate gyrus cell population, we performed a long-term (4 weeks) depletion of the neurogenic capacity, by administering cytosine arabinoside in ME7 mice (Fig. 3A). Treatment with cytosine arabinoside induced the expected depletion of the neurogenic activity at the dentate gyrus of ME7 mice, evidenced by a significant decrease in the number of BrdU+ and DCX+ cells (Fig. 3B and C), when compared with saline-treated ME7 mice. Interestingly, the depletion of neurogenesis for 4 weeks had an impact on the preservation of the dentate gyrus in ME7 mice, inducing significant degeneration of the dentate gyrus (Fig. 3D–F), when compared with the preserved integrity of saline-treated ME7 mice. Of note, cytosine arabinoside-treated ME7 mice displayed a significant reduction of the connectivity (synaptophysin staining) with the main synaptic target of the dentate gyrus, the stratum lucidum of CA3 pyramidal cells, as a consequence of the neurodegeneration, when compared with the saline-treated ME7 group (Fig. 3G and H).

Our results support the hypothesis that an increased neurogenic activity during prion disease accounts for the preservation of the dentate gyrus despite the ongoing degeneration of granule cells. The data provide evidence for a repair mechanism to counteract disease progression.

Prion disease induces aberrant differentiation of newborn neurons

As the increase in neurogenesis may lead to the protection of the dentate gyrus in prion disease, we investigated the differentiation and integration of newborn neurons (Fig. 4). We combined the tracing of newborn neurons with two γ-retroviral vectors, expressing the fluorescent proteins Venus and mCherry, to obtain information about neurons generated at different times and surviving for different times (Fig. 4A). We analysed the morphological maturation of γ-retrovirus-traced newborn neurons by performing Sholl analysis and measuring number and length of the dendrites (Fig. 4B–F). In prion disease, neurons of 4 weeks of age (Venus+) (generated at 8-week post disease induction and surviving to 12 weeks), showed a reduced ramification of the dendritic tree with a higher number of dendrites projecting a shorter distance into the molecular layer (Fig. 4B, E and F), when compared with the neurons analysed in NBH controls. This aberrant pattern of differentiation is also evident in the neurons generated at 12 weeks and surviving for 8 weeks to late disease at 20 weeks (mCherry+; Fig. 4C, E and F) and neurons generated at 12 weeks and surviving for 12 weeks until 20 weeks (Venus+; Fig. 4D–F). It is clear that the neurons generated during prion disease progression fail to achieve the full morphological complexity of mature dentate granule neurons.

We completed the study of the maturation of newborn neurons in prion disease by analysing both the dendritic and axonal compartments (Fig. 5). We observed a progressive increase in the number of dendritic spines in NBH control neurons, from 4 to 12 weeks of maturation (Fig. 5B). However, granule neurons generated during prion disease had fewer spines along the distal segment of the dendritic tree throughout the differentiation process (Fig. 5A and B). We also observed a pronounced tortuosity of the dendrites of the newborn neurons, as opposed to the straighter projection pattern observed in NBH controls (Fig. 5A). Granule neurons project their axons to the stratum lucidum of the CA3 area (mossy fibre pathway), ending in synaptic boutons that progressively increase in size during maturation (Fig. 5C and D). In prion disease, synaptic boutons show a delayed maturation program, only reaching the control size at the latest stage analysed (12-week-old neurons; Fig. 5C and D). The integrity of the mossy pathway was also evidenced by the preservation of synaptophysin staining of the large boutons in the stratum lucidum (Fig. 5E and F).

To demonstrate the preservation of the mossy pathway we performed tracing experiments with biotinylated dextran amine in the CA3 layer (Fig. 5G and H). Biotinylated dextran amine-traced dentate neurons were observed in both NBH controls and ME7 prion diseased mice, indicating the integrity of the mossy fibre projection (Fig. 5G). The detailed analysis of the traced neurons showed a lower frequency of mature neurons (characterized by large bi- or multipolar dendritic trees, with cell bodies close to the outer edge of the layer) in ME7 mice, and the overall cell morphology resembled that evidenced with retroviral tracing experiments (Fig. 4), characterized by unipolar and shorter dendritic trees

Figure 1 Continued
(short-term experiment) in the subgranular layer of the dentate gyrus of prion disease (ME7) and control (NBH) mice (see representative images, **D**). Quantified data expressed as the mean ± SEM of the number of BrdU+ cells/mm^2. (**E** and **F**) Immunohistochemical analysis of the temporal expression of DCX, calretinin and Sox2 at the subgranular layer of the dentate gyrus of prion disease (ME7; black bars) and control (NBH; open bars) mice (see representative images for DCX, **E**). Quantified data expressed as mean ± SEM of the number of DCX+, calretinin+ or Sox2+ cells/mm^2. (**G**) Confocal microscopy analysis of the incorporation of BrdU (red; short-term experiment) in DCX+ cells (green) by double immunofluorescence in the dentate gyrus of prion (ME7) or control (NBH) mice. Quantified data expressed as the mean ± SEM of the number of DCX+BrdU+ cells/mm^2. Statistical differences: $^*P < 0.05$, $^{**}P < 0.01$, $^{***}P < 0.001$. Data were analysed with a two-way ANOVA and a *post hoc* Tukey test ($n = 6$). Nuclei are stained in blue with haematoxylin and eosin (**B** and **E**) or Hoechst (**F**). Scale bars: **B** and **E** = 50 μm; **G** = 20 μm.

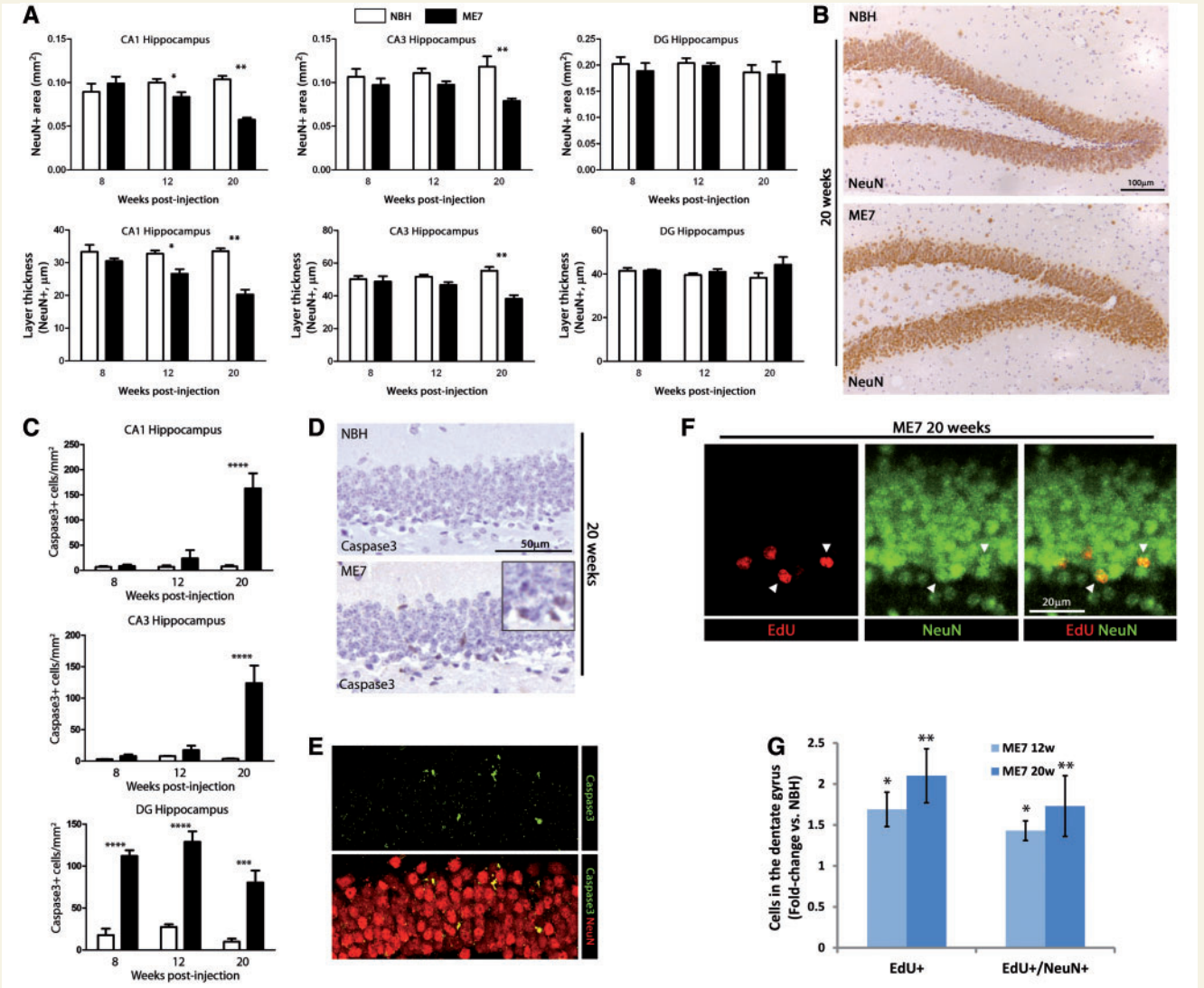

Figure 2 Increased neurogenesis in prion disease preserves the integrity of the dentate gyrus. (**A** and **B**) Morphometric analysis of the integrity of the hippocampal neuronal layers [CA1, CA3 and dentate gyrus (DG)] in prion disease (ME7; black bars) and control (NBH; open bars) mice. Quantified data expressed as mean ± SEM of the layer area (NeuN+, mm^2) or thickness (NeuN+, µm). (**B**) Representative immunostaining for NeuN in the dentate gyrus of ME7 or NBH mice. (**C** and **D**) Immunohistochemical analysis of the expression of the cleaved form of the caspase 3 in the hippocampal neuronal layers (CA1, CA3 and dentate gyrus) in prion disease (ME7; black bars) and control (NBH; open bars) mice (see representative images, **D**). Detail of apoptotic bodies and nuclear condensation is shown in (**D**; inset). Quantified data expressed as the mean ± SEM of the number of caspase 3+ cells/mm^2. (**E**) Confocal microscopy analysis of the expression of caspase 3 (green) in granule cells (NeuN+; red) by double immunofluorescence in the dentate gyrus of prion mice (ME7). (**F** and **G**) Confocal microscopy analysis of the incorporation of EdU (red; long-term experiment) in NeuN+ granule cells (green) by double immunofluorescence in the dentate gyrus of prion (ME7) or control (NBH) mice. Quantified data expressed as the mean ± SEM of the fold-change (ME7 versus NBH) of EdU+ or EdU+/NeuN+ cells in the dentate gyrus. Statistical differences: $*P < 0.05$, $**P < 0.01$, $***P < 0.001$, $****P < 0.0001$. Data were analysed with a two-way ANOVA and a *post hoc* Tukey test ($n = 4–6$). Nuclei are stained in blue with haematoxylin and eosin (**D**). Scale bars: **B** = 100 µm; **D** = 50 µm; **E** and **F** = 20 µm.

with tortuous ramifications (Fig. 5G and H). The preservation of the dentate gyrus integrity (Figs 2 and 5) was further corroborated using Golgi-stained slices from ME7 mice, in which we observed maintenance of the cellular composition of the dentate gyrus despite widespread neurodegeneration from the CA1 to CA3 layers (Fig. 5I). With the results obtained with the tracing experiments, the overall cellular composition of the dentate gyrus could be assigned to a 'rejuvenated phenotype' (smaller granule cells with shorter and more profuse dendritic arborisations), previously reported in other experimental paradigms (Danzer, 2012).

Using electron microscopy in combination with Venus immunogold staining (Fig. 6A and B), we studied the dendrites of granular neurons from NBH and ME7 animals. In both cases, the Venus+ neurons did not show differences in the dendrite cytoplasmic

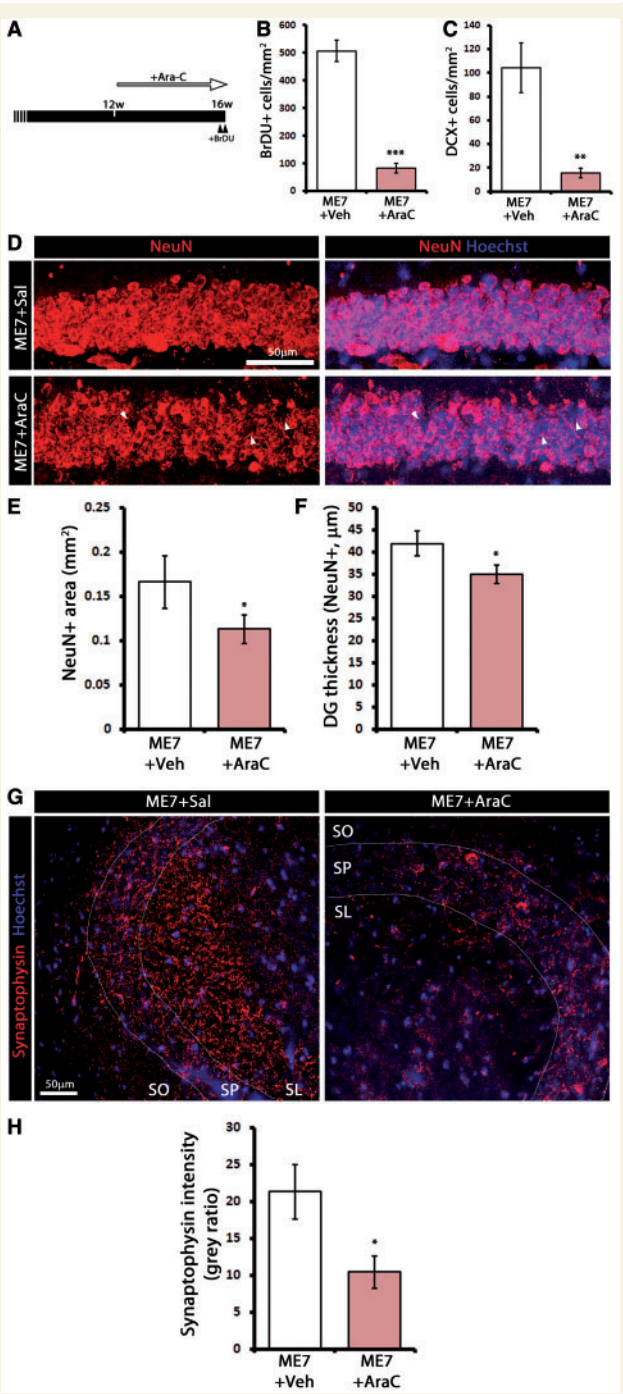

Figure 3 Depletion of neurogenesis impacts the preservation of the dentate gyrus observed in prion disease. (**A**) Neurogenesis was depleted in prion diseased mice (ME7) for 4 weeks, by the intraventricular infusion of cytosine arabinoside (Ara-C). (**B** and **C**) Immunohistochemical analysis of the incorporation of BrdU (**B**) and the expression of DCX (**C**) in the dentate gyrus of ME7 mice, treated with cytosine arabinoside (red bars) or saline (control, open bars). (**D–F**) Morphometric analysis of the integrity of the dentate gyrus in prion disease (ME7) treated with cytosine arabinoside (red bars) or saline (control, open bars). Quantified data expressed as mean ± SEM of dentate gyrus area (**E**, NeuN+, mm^2) or thickness (**F**, NeuN+, µm). Representative confocal microscopy images of the immunostaining for NeuN shown in (**D**), with arrowheads indicating cell gaps. (**G** and **H**) Immunohistochemical analysis of the expression of synaptophysin in the CA3 area of the hippocampus of ME7 mice, treated with cytosine arabinoside (red bars) or saline (control, open bars). Representative confocal microscopy images of the immunostaining for synaptophysin shown in (**G**). SO = stratum oriens; SP = stratum pyramidale; SL = stratum lucidum. (**H**) Quantified data expressed as the mean ± SEM of the intensity of fluorescence of synaptophysin (grey ratio). Statistical differences: $*P < 0.05$, $**P < 0.01$, $***P < 0.001$. Data were analysed with a *t*-test ($n = 4$). Nuclei are stained in blue with Hoescht (**E** and **H**). Scale bars: **E** and **H** = 50 µm.

content and organules. Moreover, synaptic contacts were found on NBH (Fig. 6C) and ME7 derived neurons (Fig. 6D), indicating that there was a correct development of the synaptic contacts.

Our results show that chronic neurodegeneration induces an effective neurogenic response in the subgranular layer, which plays a role in rejuvenating the dentate gyrus and maintaining the connectivity with CA3, but the ongoing neurodegenerative process compromises the dendritic differentiation.

Newborn granule cells in prion disease have normal electrophysiological properties but older neurons show increased excitability

We next explored whether the basic functional characteristics of newly generated and older granule cells are different in NBH and ME7 animals. To this end, we performed electrophysiological recordings. We saw that there were no differences in resting membrane potential, or action potential threshold in all groups tested when comparing by treatment (NBH versus ME7) or cell type (Venus+ versus older) (Supplementary Table 2).

Previous studies have shown three main groups of granule neurons in normal mice with high (>2000 MΩ), intermediate, and low (<500 MΩ) input resistance (R_i), which becomes progressively lower as granule cells mature (Liu *et al.*, 2000; Schmidt-Hieber *et al.*, 2004). Consistent with these reports, we saw a trend for higher R_i in newly generated neurons (Fig. 7A). However, our R_i results had a large variability (e.g. NBH Venus+ mean: 1885 ± 501 MΩ, $n = 11$), likely indicating that this group incorporates neurons from both high and intermediate R_i whereas the non-labelled neurons had a much lower input resistance (e.g. non-labelled neurons 499 ± 99 MΩ, $n = 6$), meaning that they are of an older age as none of these had R_i >1000 MΩ (Fig. 7A).

To test whether 4-week-old neurons in prion mice at 18 weeks post-induction have the same degree of excitability we applied square current pulses of increasing amplitude and tested the current amplitude at which the first action potential was elicited (Fig. 7B). As expected from previous work (Schmidt-Hieber *et al.*, 2004) we saw that younger labelled neurons in control NBH mice were more excitable and required less current to fire action potentials (Fig. 7B and C). Interestingly, this was also the case for labelled neurons in prion mice, showing that they have the same

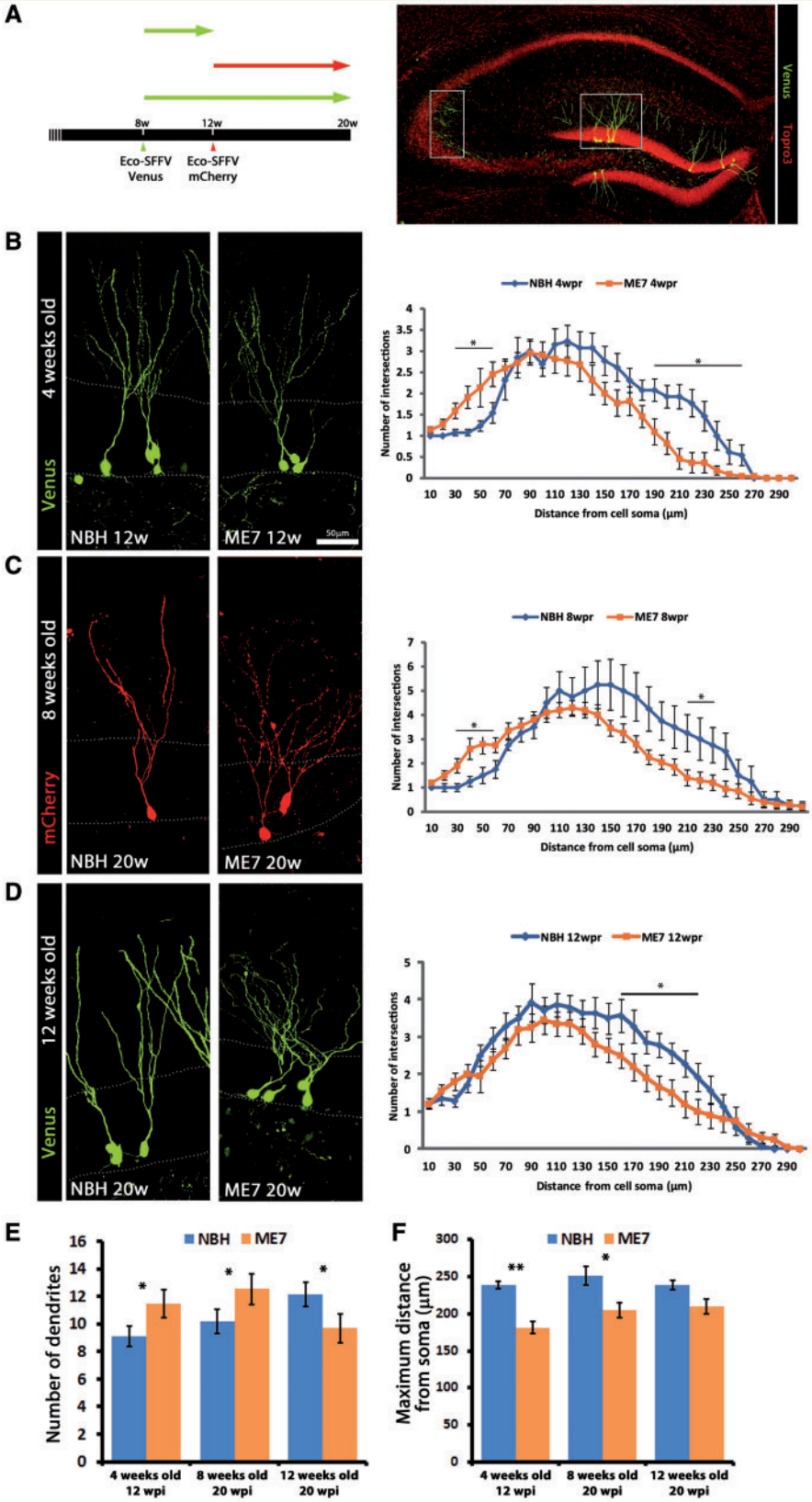

Figure 4 Impaired maturation of granule cells during prion disease. (**A**) Sequential bi-colour marking of neuron generation in the dentate gyrus by the intraparenchymal (hilus) administration of ecotropic SFFV γ-retroviral (Eco-SFFV-RV) vectors (see experimental scheme, *left*), in ME7 or NBH mice. Neurons traced with γ-retrovectors were analysed for the maturation of their dendritic tree, the generation of dendritic spines (Fig. 5) and the maturation of synaptic boutons connecting with the CA3 layer (Fig. 5). (**B–D**) Projection of confocal z-stacks of Venus + 4-week-old, mCherry + 8-week-old, or Venus + 12-week-old granule neurons from NBH or ME7 mice

(continued)

degree of excitability as young neurons from control mice. Furthermore, as expected, higher current amplitude was necessary to elicit action potentials in older neurons in control mice. However, in prion mice older neurons were strikingly more excitable, producing action potentials in response to smaller current pulses [ANOVA revealed a treatment–cell type interaction $F(1,17) = 9.69$, $P < 0.01$; Fig. 7B and C]. These data show that the intrinsic properties of newly generated neurons are similar between control and prion mice, however ME7 neurons become hyperexcitable as they mature.

Hippocampal neurogenesis is increased in human Alzheimer's disease and variant Creutzfeldt-Jakob's disease

As a final objective, we analysed the degree of similarity of the observed changes in neurogenesis in the model of prion disease with those present in two human neurodegenerative diseases: variant CJD, a human form of prion disease, and Alzheimer's disease (Fig. 8 and Supplementary Table 4). We first observed preservation of the number of cells of the dentate gyrus (Fig. 8A). Both patients with variant CJD and those with Alzheimer's disease show increased cell proliferation at the subgranular layer of the dentate gyrus, evidenced by immunostaining for Ki67 (Fig. 8B and E). Ki67+ cells in the dentate gyrus were found to be non-microglial cells (Supplementary Fig. 3). The pool of neural stem cells (Sox2+; Fig. 8C and G) remains unchanged in variant CJD or Alzheimer's disease tissue, whereas the population of neural precursor cells (calretinin+) is increased in both variant CJD and Alzheimer's disease brains (Fig. 8D and F). This immunohistochemical analysis also indicates a decreased neurogenic activity related to ageing, evidenced by the difference seen in the age-matched control groups (variant CJD controls, Alzheimer's disease controls).

These results indicate that the changes observed in the experimental model of prion disease were similarly present in human variant CJD and Alzheimer's disease brain tissue, where we observed an enhanced neurogenic response, suggesting that this model may shed light on the processes of adult neurogenesis during chronic neurodegeneration.

Discussion

Although the study of neurogenesis in the subgranular layer or subventricular zone during neurodegenerative disorders in animal models and humans has been a major focus of interest in past years, no clear, common and universal mechanisms of regulation have been described, in no small part due to the heterogeneity of the experimental conditions used (for review see Winner *et al.*, 2011). The model of prion disease provides a unique approach to study the early and late impact of the chronic and progressive neurodegenerative events that could influence the regulation of neurogenesis (Supplementary Fig. 4). Our results indicate that prion disease has a profound impact on the regulation of the adult hippocampal neurogenic niche, causing an initial rapid increase in the generation of neural precursors, followed by an aberrant maturation and integration into the pre-existing circuitry (Supplementary Fig. 4). The generation of newborn neurons is translated into maintaining the dentate gyrus integrity, in contrast to the degeneration and destruction observed both in CA1 and CA3 layers of the hippocampus, regions that do not benefit from any neuronal replacement. A similar mechanism could take place in human Alzheimer's disease and variant CJD, as our results could be interpreted as increased neurogenic activity at the dentate gyrus in these diseased human brains, in line with previously reported data (Jin *et al.*, 2004). The analysis of newborn neurons using tracing with γ-retroviral vectors, tracing with biotinylated dextran amine and Golgi-Cox staining lead us to the concept of a 'partial rejuvenation' process of the dentate gyrus during prion disease. The observed phenotype of new neurons in prion disease has been previously described in various experimental models of Alzheimer's disease (Li *et al.*, 2009; Sun *et al.*, 2009; Llorens-Martin *et al.*, 2013) or in post-mortem human Alzheimer's disease tissue (Llorens-Martin *et al.*, 2013). However, as this fatal prion disease progresses to later stages the earlier increase in neurogenic response declines, indicating its failure at terminal stages. Therefore, our data suggest a biphasic model of regulation of neurogenesis in chronic neurodegeneration, previously proposed as possible for Alzheimer's disease (Waldau and Shetty, 2008), explaining the controversy in the field and providing a unifying response to the question 'Is neurogenesis up- or down-regulated in neurodegeneration?' It is likely both, depending on the time examined during disease progression.

Although the initial neurogenic wave supports the preservation of the integrity of the dentate gyrus, we found interesting evidence of the neurogenic process failing at later or terminal stages of the disease, as the increase in DCX+ cells in the dentate gyrus is not observed at terminal points. We propose that there may be two main scenarios happening at the later stages of the disease, when widespread neurodegeneration translates into clinical symptoms. First, prion disease could be affecting the survival of newly generated neural precursor cells such that they are disabled, and unable to reach the immature stage of differentiation (DCX+). This idea is supported by the fact that PrP^c, the constitutive form of the prion protein, is expressed in newly formed neurons, but is not present in either neural stem cells or glial precursor cells (Steele *et al.*, 2006). Misfolding of PrP^c, required for the

Figure 4 Continued
(see experimental scheme, **A**). The maturation of the dendritic trees was analysed according to the Sholl method (**B–D**, *right*), representing the mean ± SEM of the number of intersections at increasing distances from the cell soma. (**E**) Quantification of the total number of dendrites/neuron, in cells traced as described previously (**A**), expressed as mean ± SEM. (**F**) Quantification of the maximum distance from cell soma, in cells traced as described previously (**A**), expressed as mean ± SEM (μm). Statistical differences: $*P < 0.05$, $**P < 0.01$. Data were analysed with a *t*-test. Scale bar: **B–D** = 50 μm. wpr = week post-retrovirus.

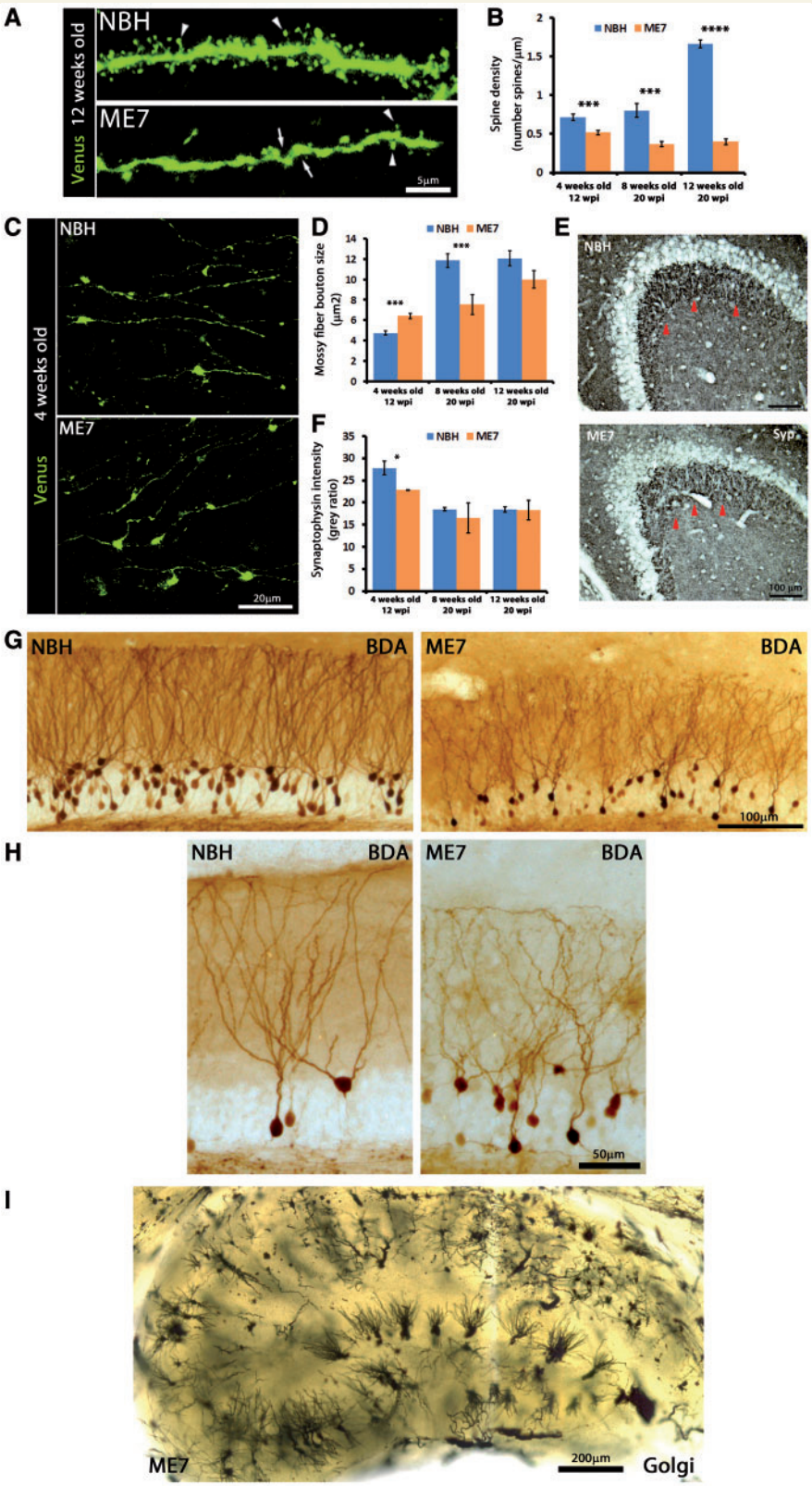

Figure 5 Impaired connectivity of granule cells during prion disease. (**A–D**) Neurons traced with γ-retrovectors, with 4, 8 or 12 weeks of age (see Fig. 4), were analysed for the generation of dendritic spines (**A** and **B**) and the maturation of synaptic boutons connecting with the CA3 layer (**C** and **D**), in both NBH and ME7 mice. Projection of confocal *z*-stacks of the terminal dendritic segment of Venus+ 12-week-old granule neurons from NBH or ME7 mice, evidencing the number and morphology of dendritic spines (arrowheads) and the morphology of the ramification (arrows). (**B**) Dendritic spines were quantified in the distal 100 μm of the dendrite, and data is presented as mean ± SEM of the number of spines/μm. (**C**) Projection of confocal *z*-stacks of the terminal dendritic segment of Venus+ 4-week-old

(continued)

generation of the toxic form(s) PrPSc, could be indirectly targeting the population of early neural cells, which may be especially vulnerable due to a lack of trophic support provided by sufficient and functional synaptic connections (Doetsch and Hen, 2005). This idea is supported by recent evidence of the generation of PrPSc in cultured neural stem cells derived from ME7 mice, and its effects on their fate choice (Relano-Gines *et al.*, 2013). Second, the correct targeting of synaptic input from the afferent connections is crucial for the proliferation and integration of newborn neurons into the dentate gyrus (Vivar *et al.*, 2012; Perederiy *et al.*, 2013). Newborn granule cells initially receive afferents from intra-hippocampal cells and septal cholinergic cells, before receiving progressive input from distal lateral entorhinal cortex (Vivar *et al.*, 2012; Deshpande *et al.*, 2013). At early stages of cell development, tonic activation of $GABA_A$ receptors by ambient GABA regulates neuronal differentiation of hippocampal progenitor cells (Tozuka *et al.*, 2005) and dendritic growth of newborn granular cells

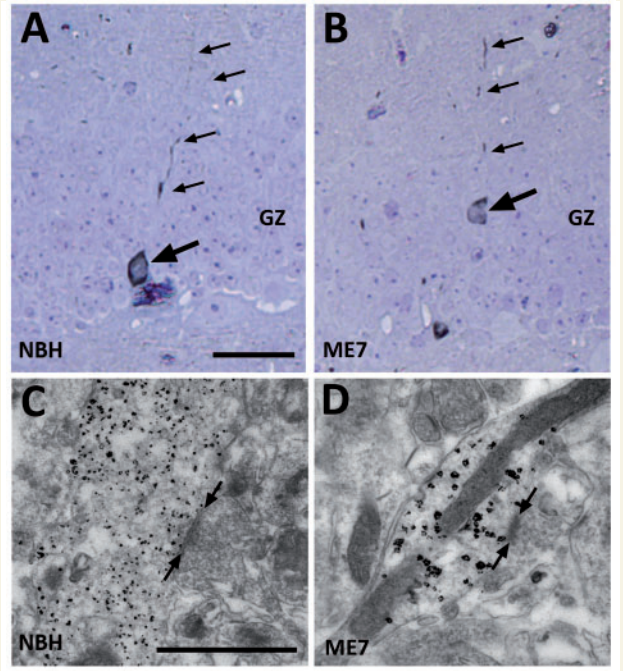

Figure 6 Characterization of newborn granular dendrites by transmission electron microscopy. Pre-embedding immunogold detection of Venus in the dentate gyrus, after γ-retroviral tracing. (**A** and **B**) Toluidine blue-stained semithin sections showing black immunogold–silver labeling for Venus in NBH and ME7 granular neurons. (**C** and **D**) Transmission electron microsopy details of the immunogold-labeled neuronal dendrites showing dendritic synapses. Scale bars: **A** and **B** = 25 μm; **C** and **D** = 1 μm.

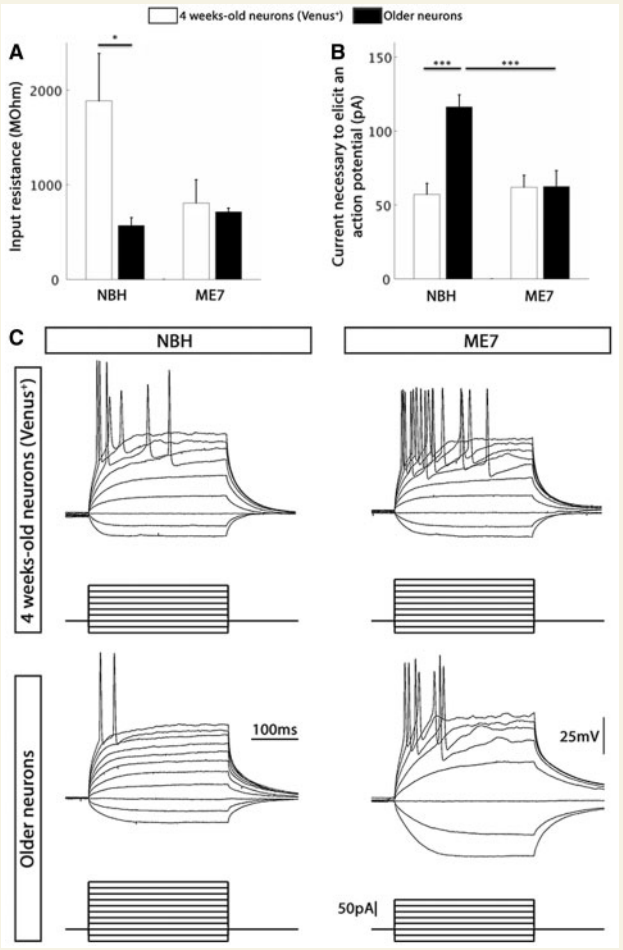

Figure 7 Electrophysiological properties of granule cells from NBH and ME7 mice. (**A**) Summary of R_i measures in neurons. (**B**) Summary of current pulse amplitude necessary to elicit an action potential. (**C**) Examples of neuronal responses (*top* traces) observed by applying square current pulses of increasing amplitude (*bottom* traces). Four-week-old granule cells (Venus+; open bars) or older granule cells (Venus-; black bars) were analysed in hippocampal slices after γ-retroviral tracing. $^*P < 0.05$, $^{**}P < 0.01$, significant differences Student's *t*-test using *post hoc* Dunn-Šidák correction.

Figure 5 Continued
granule neurons from NBH or ME7 mice, evidencing the morphology of the synaptic boutons of the mossy fibres. (**D**) Mossy fibre boutons size was quantified and data is presented as mean ± SEM of the bouton size (μm^2). (**E** and **F**) Immunohistochemical analysis of the expression of synaptophysin in the CA3 area of the hippocampus of NBH or ME7 mice (stratum lucidum limited by red arrows). (**F**) Quantified data expressed as the mean ± SEM of the intensity of synaptophysin staining (grey ratio). (**G** and **H**) Retrograde tracing with biotinylated dextran amine (injected at CA3 layer) of dentate neurons in NBH and ME7 mice [16 weeks post-induction (wpi)], evidencing the integrity of the mossy fibre connection, the morphology of the granule cells and their dendritic trees (**H**). (**I**) Representative image of a Golgi-stained hippocampal slice from ME7 mice. Statistical differences: $^*P < 0.05$, $^{***}P < 0.001$, $^{****}P < 0.0001$. Data were analysed with a *t*-test (in **E** and **F**). Scale bars: **A** = 5 μm; **C** = 20 μm; **E** and **G** = 100 μm; **H** = 50 μm; **I** = 200 μm.

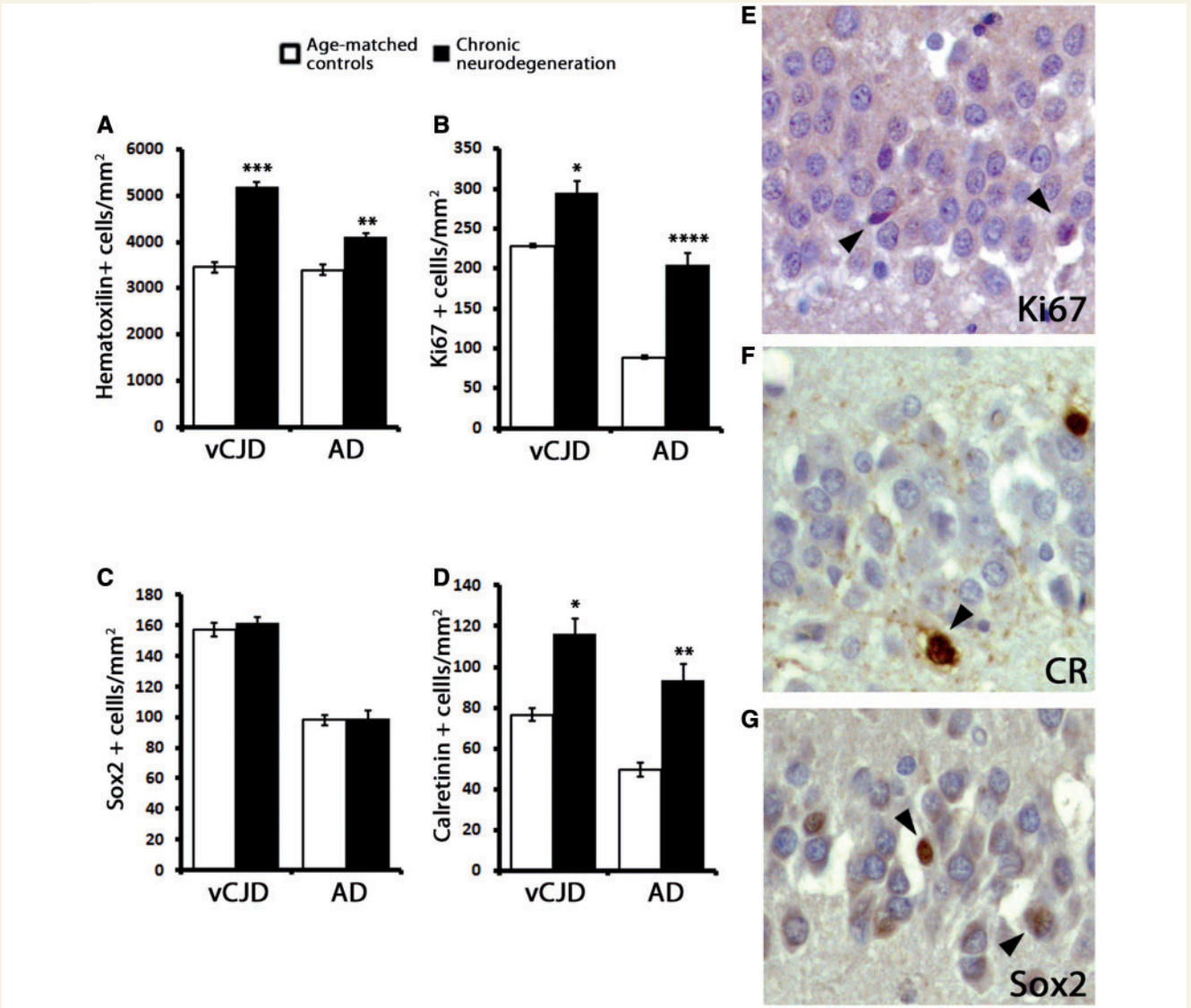

Figure 8 Hippocampal neurogenesis in variant Creutzfeldt–Jakob disease and Alzheimer's disease. Histochemical analysis of the number of cells of the dentate gyrus (**A**) and the expression of Ki67 (marker of proliferation; **B**), Sox2 (marker of neural stem cells; **C**) and calretinin (marker of neural progenitors; **D**) in the dentate gyrus of variant CJD (vCJD) and Alzheimer's disease (AD) brains, compared with age-matched controls (representative images shown in **E–G**). Nuclei are stained with haematoxylin and eosin (blue). Quantification data expressed as mean ± SEM of the number of haematoxylin+ (**A**), Ki67+ (**B**), Sox2+ (**C**) or Calretinin+ (**D**) cells/mm^2. Statistical differences: $*P < 0.05$, $**P < 0.01$, $***P < 0.001$, $****P < 0.0001$, expressed versus the correspondent age-matched control. Data were analysed with a two-way ANOVA and a *post hoc* Tukey test ($n = 9–10$).

(Ge *et al.*, 2008). Later, stimulation of glutamate receptors becomes critical in shaping the plasticity of adult-born granule cells (Tashiro *et al.*, 2006). Because neurodegeneration is closely associated with aberrant excitatory and inhibitory activity (Palop *et al.*, 2007), we hypothesize that prion disease could be affecting adult neurogenesis by altering the balance between excitatory and inhibitory inputs onto adult-born neurons in the dentate gyrus. These events have been recently reported to be crucial for the integration of newborn neurons in models of Alzheimer's disease (Li *et al.*, 2009; Sun *et al.*, 2009). Among the observed morphological deficits of newborn neurons in prion disease, a remarkable decrease in the number of apical dendritic spines could reflect defective connectivity with the main afferent input from the entorhinal cortex. There is evidence supporting an early impact on the entorhinal cortex in experimental models of prion disease (Cunningham *et al.*, 2003), although more detailed tracing studies are needed to better analyse the hypothesis of an initial damage of the entorhinal cortex being causative for the changes observed at the dentate gyrus.

There is an emerging interest on the possibility of dentate gyrus neural stem cells being end-state glia. Recent reports point to a limited renewal and proliferative capacity of neural stem cells in the dentate gyrus (Encinas *et al.*, 2011) related to the reported age-related decline in neurogenesis (Kuhn *et al.*, 1996).

Thus, there would be only a limited pool of neural stem cells, designed to provide neurogenic physiological support to the dentate gyrus (for review see Bonaguidi *et al.*, 2012). During pathological events, acceleration of neural stem cells or neural precursors proliferation could be expending the neurogenic potential during early stages of the disease, balancing neuronal loss but compromising the final outcome. Alternatively, neural stem cells could serve as an intermediate stage towards the generation of new neurons and glia. The existence of silent or quiescent stem cells, or cells with the potential to become stem cells, has been supported by experimental evidence in both the olfactory bulb and subventricular zone levels (Leung *et al.*, 2007; Coskun *et al.*, 2008; Carlen *et al.*, 2009). Also, a recent report describes a population of quiescent neural stem cells in the dentate gyrus, activated 'on demand' during physical exercise or seizures (Lugert *et al.*, 2010). In our model, we observe a dramatic increase in neurogenesis during the early and mid-stages of the prion disease, which is not maintained at later stages of disease. Thus, prion diseased animals could be experiencing an accelerated neurogenic response, to compensate for the observed neuronal damage at early stages, but this will exhaust the self-replacement mechanism while responding to the inexorable progression of the disease process. If, in contrast, the increased neurogenic response is not exhausting the neural stem cells pool (as suggested by our Sox2 data), we could be facing a mechanism driving a significant increase of neurogenesis without any impact on the neurogenic reservoir, which would have a clear impact for potential repair strategies. The observed self-repairing response would not work at the expense of the pool of radial progenitors, bypassing the age-dependent 'deforestation' of the neural stem cells (Encinas *et al.*, 2011). Therefore, the use of pro-neurogenic therapies or approaches aimed at reactivating the proliferation of neural stem cells would restore the observed decline in neurogenesis at late stages of disease, providing a longer lasting repair response. In this line, evidence supports that environmental enrichment and/or enhanced physical activity rescues the decay in adult neurogenesis and cognitive decline observed in transgenic models of Alzheimer's disease (Cracchiolo *et al.*, 2007; Valero *et al.*, 2011; Marlatt *et al.*, 2013). Analysing the dynamics of the neural stem cells pool during prion disease would therefore be very informative and a matter for future studies. Future studies aimed at rescuing the neurogenic response at late stages of prion disease (i.e. combining with environmental enrichment and/or physical activity) would be also informative to better weight the real contribution of hippocampal neurogenesis to the progression and outcome of prion disease.

Inflammation may play an important role in the regulation of neurogenesis during the prion pathology. There is increasing evidence implicating microglia in the active regulation of adult neurogenesis (Gebara *et al.*, 2013). Under basal conditions, apoptotic corpses of newly generated neurons are rapidly phagocytosed from the niche by resident microglia in the adult subgranular zone (Sierra *et al.*, 2010). Under inflammatory conditions, activated microglia can have both beneficial and detrimental effects on different aspects of adult neurogenesis, depending on the balance between secreted molecules with pro- and anti-inflammatory actions (for review see Ekdahl *et al.*, 2009). Recently, we have been able to demonstrate that prion disease is characterized by a massive expansion of the population of microglial cells, generated by local proliferation, and they have a net deleterious contribution to the pathology (Gomez-Nicola *et al.*, 2013). Thus, the proliferative and inflammatory reaction in microglial cells residing within the dentate gyrus of prion diseased animals could be intimately related to the neurogenic events. Further experimental analysis will be necessary to provide insight into this hypothesis, but again the prion model will continue to be a valuable model for the study of these events during chronic neurodegeneration.

As a consequence of the accelerated replacement of granule cells, neurons with young or immature phenotypes become abundant in the dentate gyrus, as previously described for other pathological conditions such as epilepsy (Danzer, 2012). A shift in the balance of young versus old granule neurons in the dentate gyrus could impact the maintenance of key memory functions, such as pattern separation and completion (Nakashiba *et al.*, 2012). Our results show that both new and older neurons in ME7 animals have physiologically healthy resting membrane potentials, and have active membrane properties that can sustain action potential generation. Furthermore all neurons received synaptic input as measured in voltage clamp experiments (data not shown). This means that these neurons are incorporated into the hippocampal network circuit. Consistent with previous work (Liu *et al.*, 2000; Schmidt-Hieber *et al.*, 2004), our results show that newly generated neurons are more excitable than older neurons in NBH mice. It has been shown that this higher likelihood to produce action potentials provides new granule cells with enhanced synaptic plasticity (Schmidt-Hieber *et al.*, 2004), which may be crucial for their maturation and participation in hippocampal memory functions (Jung and McNaughton, 1993; Skaggs *et al.*, 1996). In prion mice, newly generated neurons, and surprisingly, older neurons were highly excitable. However, more experimental work is needed to test whether their synaptic input and plasticity matches that of new neurons in NBH mice, and whether they possess other intrinsic properties specific to young neurons such as the presence of T-type Ca^{2+} channels which can boost fast Na^{+} action potentials. The enhanced excitability of older neurons in prion mice may lead to aberrant activity, such as the EEG patterns observed in variant CJD cases (Ferrer *et al.*, 1993; Lapergue *et al.*, 2010) or experimental mice (Bassant *et al.*, 1984; Jefferys *et al.*, 1994) interfering with memory mechanisms (Jung and McNaughton, 1993; Skaggs *et al.*, 1996), such as the impairments described in this model of prion disease (Cunningham *et al.*, 2003).

In summary, our data provide a novel and detailed analysis of the hippocampal neurogenic response in a model of chronic and fatal neurodegeneration, prion disease. These results and the advantages of the study of experimental models of prion disease served to provide valuable insights into the understanding of the self-repairing mechanisms of the degenerating brain (Supplementary Fig. 4). Our proposed biphasic model of neurogenesis in chronic neurodegeneration would explain the discrepancies found among different studies and would highlight a critical period for the promotion of targeted repair strategies during chronic neurodegeneration. Therefore, a better understanding of the preclinical, latent phase of the disease in humans and models like prion disease would provide a way of defining the optimal

time for the evaluation of therapeutic approaches to promote neurogenesis.

Acknowledgements

We thank the National CJD Surveillance Unit Brain Bank (Edinburgh, UK) for the provision of human brain tissue samples. We thank Chrysia-Maria Pegasiou for technical assistance. FACS analysis was performed in the FACS Core Facility of the UMC Hamburg-Eppendorf.

Funding

The research was funded by the European Union Seventh Framework Programme under grant agreement IEF273243, by a postdoctoral fellowship from the MEC (Spain), by the MRC (MR/K022687/1) and the DFG (SFB841, project SP2).

Supplementary material

Supplementary material is available at *Brain* online.

References

Alvarez-Buylla A, Seri B, Doetsch F. Identification of neural stem cells in the adult vertebrate brain. Brain Res Bull 2002; 57: 751–8.

Arvidsson A, Collin T, Kirik D, Kokaia Z, Lindvall O. Neuronal replacement from endogenous precursors in the adult brain after stroke. Nat Med 2002; 8: 963–70.

Bassant MH, Cathala F, Court L, Gourmelon P, Hauw JJ. Experimental scrapie in rats: first electrophysiological observations. Electroencephalogr Clin Neurophysiology 1984; 57: 541–7.

Baum C, Itoh K, Meyer J, Laker C, Ito Y, Ostertag W. The potent enhancer activity of the polycythemic strain of spleen focus-forming virus in hematopoietic cells is governed by a binding site for Sp1 in the upstream control region and by a unique enhancer core motif, creating an exclusive target for PEBP/CBF. J Virol 1997; 71: 6323–31.

Behrens A, Brandner S, Genoud N, Aguzzi A. Normal neurogenesis and scrapie pathogenesis in neural grafts lacking the prion protein homologue Doppel. EMBO Rep 2001; 2: 347–52.

Boekhoorn K, Joels M, Lucassen PJ. Increased proliferation reflects glial and vascular-associated changes, but not neurogenesis in the presenile Alzheimer hippocampus. Neurobiol Dis 2006; 24: 1–14.

Bonaguidi MA, Song J, Ming GL, Song H. A unifying hypothesis on mammalian neural stem cell properties in the adult hippocampus. Curr Opin Neurobiol 2012; 22: 754–61.

Carlen M, Meletis K, Goritz C, Darsalia V, Evergren E, Tanigaki K, et al. Forebrain ependymal cells are Notch-dependent and generate neuroblasts and astrocytes after stroke. Nat Neurosci 2009; 12: 259–67.

Coskun V, Wu H, Blanchi B, Tsao S, Kim K, Zhao J, et al. CD133+ neural stem cells in the ependyma of mammalian postnatal forebrain. Proc Natl Acad Sci USA 2008; 105: 1026–31.

Cracchiolo JR, Mori T, Nazian SJ, Tan J, Potter H, Arendash GW. Enhanced cognitive activity—over and above social or physical activity—is required to protect Alzheimer's mice against cognitive impairment, reduce Abeta deposition, and increase synaptic immunoreactivity. Neurobiol Learn Mem 2007; 88: 277–94.

Cunningham C, Deacon R, Wells H, Boche D, Waters S, Diniz CP, et al. Synaptic changes characterize early behavioural signs in the ME7 model of murine prion disease. Eur J Neurosci 2003; 17: 2147–55.

Danzer SC. Depression, stress, epilepsy and adult neurogenesis. Exp Neurol 2012; 233: 22–32.

Deshpande A, Bergami M, Ghanem A, Conzelmann KK, Lepier A, Gotz M, et al. Retrograde monosynaptic tracing reveals the temporal evolution of inputs onto new neurons in the adult dentate gyrus and olfactory bulb. Proc Natl Acad Sci USA 2013; 110: E1152–61.

Doetsch F, Garcia-Verdugo JM, Alvarez-Buylla A. Regeneration of a germinal layer in the adult mammalian brain. Proc Natl Acad Sci USA 1999; 96: 11619–24.

Doetsch F, Hen R. Young and excitable: the function of new neurons in the adult mammalian brain. Curr Opin Neurobiol 2005; 15: 121–8.

Ekdahl CT, Kokaia Z, Lindvall O. Brain inflammation and adult neurogenesis: the dual role of microglia. Neuroscience 2009; 158: 1021–9.

Encinas JM, Michurina TV, Peunova N, Park JH, Tordo J, Peterson DA, et al. Division-coupled astrocytic differentiation and age-related depletion of neural stem cells in the adult hippocampus. Cell Stem Cell 2011; 8: 566–79.

Ferrer I, Casas R, Rivera R. Parvalbumin-immunoreactive cortical neurons in Creutzfeldt-Jakob disease. Ann Neurol 1993; 34: 864–6.

Ge S, Sailor KA, Ming GL, Song H. Synaptic integration and plasticity of new neurons in the adult hippocampus. J Physiol 2008; 586: 3759–65.

Gebara E, Sultan S, Kocher-Braissant J, Toni N. Adult hippocampal neurogenesis inversely correlates with microglia in conditions of voluntary running and aging. Front Neurosci 2013; 7: 145.

Gomez-Nicola D, Fransen NL, Suzzi S, Perry VH. Regulation of microglial proliferation during chronic neurodegeneration. J Neurosci 2013; 33: 2481–93.

Gomez-Nicola D, Schetters ST, Hugh Perry V. Differential role of CCR2 in the dynamics of microglia and perivascular macrophages during prion disease. Glia 2014; 62: 1041–52.

Gomez-Nicola D, Valle-Argos B, Pallas-Bazarra N, Nieto-Sampedro M. Interleukin-15 regulates proliferation and self-renewal of adult neural stem cells. Mol Biol Cell 2011; 22: 1960–70.

Gomez-Nicola D, Valle-Argos B, Pita-Thomas DW, Nieto-Sampedro M. Interleukin 15 expression in the CNS: blockade of its activity prevents glial activation after an inflammatory injury. Glia 2008; 56: 494–505.

Jefferys JG, Empson RM, Whittington MA, Prusiner SB. Scrapie infection of transgenic mice leads to network and intrinsic dysfunction of cortical and hippocampal neurones. Neurobiol Dis 1994; 1: 25–30.

Jin K, Peel AL, Mao XO, Xie L, Cottrell BA, Henshall DC, et al. Increased hippocampal neurogenesis in Alzheimer's disease. Proc Natl Acad Sci USA 2004; 101: 343–7.

Jung MW, McNaughton BL. Spatial selectivity of unit activity in the hippocampal granular layer. Hippocampus 1993; 3: 165–82.

Kuhn HG, Dickinson-Anson H, Gage FH. Neurogenesis in the dentate gyrus of the adult rat: age-related decrease of neuronal progenitor proliferation. J Neurosci 1996; 16: 2027–33.

Lapergue B, Demeret S, Denys V, Laplanche JL, Galanaud D, Verny M, et al. Sporadic Creutzfeldt-Jakob disease mimicking nonconvulsive status epilepticus. Neurology 2010; 74: 1995–9.

Leung CT, Coulombe PA, Reed RR. Contribution of olfactory neural stem cells to tissue maintenance and regeneration. Nat Neurosci 2007; 10: 720–6.

Li G, Bien-Ly N, Andrews-Zwilling Y, Xu Q, Bernardo A, Ring K, et al. GABAergic interneuron dysfunction impairs hippocampal neurogenesis in adult apolipoprotein E4 knockin mice. Cell Stem Cell 2009; 5: 634–45.

Liu X, Tilwalli S, Ye G, Lio PA, Pasternak JF, Trommer BL. Morphologic and electrophysiologic maturation in developing dentate gyrus granule cells. Brain Res 2000; 856: 202–12.

Llorens-Martin M, Fuster-Matanzo A, Teixeira CM, Jurado-Arjona J, Ulloa F, Defelipe J, et al. GSK-3beta overexpression causes reversible alterations on postsynaptic densities and dendritic morphology of hippocampal granule neurons *in vivo*. Mol Psychiatry 2013; 18: 451–60.

Lugert S, Basak O, Knuckles P, Haussler U, Fabel K, Gotz M, et al. Quiescent and active hippocampal neural stem cells with distinct morphologies respond selectively to physiological and pathological stimuli and aging. Cell Stem Cell 2010; 6: 445–56.

Marlatt MW, Lucassen PJ. Neurogenesis and Alzheimer's disease: biology and pathophysiology in mice and men. Curr Alzheimer Res 2010; 7: 113–25.

Marlatt MW, Potter MC, Bayer TA, van Praag H, Lucassen PJ. Prolonged running, not fluoxetine treatment, increases neurogenesis, but does not alter neuropathology, in the 3xTg mouse model of Alzheimer's disease. Curr Top Behav Neurosci 2013; 15: 313–40.

Masters CL, Richardson EP Jr. Subacute spongiform encephalopathy (Creutzfeldt-Jakob disease). The nature and progression of spongiform change. Brain 1978; 101: 333–44.

Morita S, Kojima T, Kitamura T. Plat-E: an efficient and stable system for transient packaging of retroviruses. Gene Ther 2000; 7: 1063–6.

Nakashiba T, Cushman JD, Pelkey KA, Renaudineau S, Buhl DL, McHugh TJ, et al. Young dentate granule cells mediate pattern separation, whereas old granule cells facilitate pattern completion. Cell 2012; 149: 188–201.

Palop JJ, Chin J, Roberson ED, Wang J, Thwin MT, Bien-Ly N, et al. Aberrant excitatory neuronal activity and compensatory remodeling of inhibitory hippocampal circuits in mouse models of Alzheimer's disease. Neuron 2007; 55: 697–711.

Parent JM, Vexler ZS, Gong C, Derugin N, Ferriero DM. Rat forebrain neurogenesis and striatal neuron replacement after focal stroke. Ann Neurol 2002; 52: 802–13.

Perederiy JV, Luikart BW, Washburn EK, Schnell E, Westbrook GL. Neural injury alters proliferation and integration of adult-generated neurons in the dentate gyrus. J Neurosci 2013; 33: 4754–67.

Perry VH. Contribution of systemic inflammation to chronic neurodegeneration. Acta Neuropathol 2010; 120: 277–86.

Relano-Gines A, Gabelle A, Hamela C, Belondrade M, Casanova D, Mourton-Gilles C, et al. Prion replication occurs in endogenous adult neural stem cells and alters their neuronal fate: involvement of endogenous neural stem cells in prion diseases. PLoS Pathog 2013; 9: e1003485.

Rupp NJ, Wegenast-Braun BM, Radde R, Calhoun ME, Jucker M. Early onset amyloid lesions lead to severe neuritic abnormalities and local, but not global neuron loss in APPPS1 transgenic mice. Neurobiol Aging 2011; 32: 2324. e1–6.

Schambach A, Bohne J, Chandra S, Will E, Margison GP, Williams DA, et al. Equal potency of gammaretroviral and lentiviral SIN vectors for expression of O6-methylguanine-DNA methyltransferase in hematopoietic cells. Mol Ther 2006a; 13: 391–400.

Schambach A, Mueller D, Galla M, Verstegen MM, Wagemaker G, Loew R, et al. Overcoming promoter competition in packaging cells improves production of self-inactivating retroviral vectors. Gene Ther 2006b; 13: 1524–33.

Schmidt-Hieber C, Jonas P, Bischofberger J. Enhanced synaptic plasticity in newly generated granule cells of the adult hippocampus. Nature 2004; 429: 184–7.

Schmitz C, Rutten BP, Pielen A, Schafer S, Wirths O, Tremp G, et al. Hippocampal neuron loss exceeds amyloid plaque load in a transgenic mouse model of Alzheimer's disease. Am J Pathol 2004; 164: 1495–502.

Sholl DA. Dendritic organization in the neurons of the visual and motor cortices of the cat. J Anat 1953; 87: 387–406.

Sierra A, Encinas JM, Deudero JJ, Chancey JH, Enikolopov G, Overstreet-Wadiche LS, et al. Microglia shape adult hippocampal neurogenesis through apoptosis-coupled phagocytosis. Cell Stem Cell 2010; 7: 483–95.

Skaggs WE, McNaughton BL, Wilson MA, Barnes CA. Theta phase precession in hippocampal neuronal populations and the compression of temporal sequences. Hippocampus 1996; 6: 149–72.

Steele AD, Emsley JG, Ozdinler PH, Lindquist S, Macklis JD. Prion protein (PrPc) positively regulates neural precursor proliferation during developmental and adult mammalian neurogenesis. Proc Natl Acad Sci USA 2006; 103: 3416–21.

Sun B, Halabisky B, Zhou Y, Palop JJ, Yu G, Mucke L, et al. Imbalance between GABAergic and Glutamatergic Transmission Impairs Adult Neurogenesis in an Animal Model of Alzheimer's Disease. Cell Stem Cell 2009; 5: 624–33.

Tashiro A, Sandler VM, Toni N, Zhao C, Gage FH. NMDA-receptor-mediated, cell-specific integration of new neurons in adult dentate gyrus. Nature 2006; 442: 929–33.

Toni N, Laplagne DA, Zhao C, Lombardi G, Ribak CE, Gage FH, et al. Neurons born in the adult dentate gyrus form functional synapses with target cells. Nat. Neurosci 2008; 11: 901–7.

Tozuka Y, Fukuda S, Namba T, Seki T, Hisatsune T. GABAergic excitation promotes neuronal differentiation in adult hippocampal progenitor cells. Neuron 2005; 47: 803–15.

Valero J, Espana J, Parra-Damas A, Martin E, Rodriguez-Alvarez J, Saura CA. Short-term environmental enrichment rescues adult neurogenesis and memory deficits in APP(Sw,Ind) transgenic mice. PloS One 2011; 6: e16832.

Veenman CL, Reiner A, Honig MG. Biotinylated dextran amine as an anterograde tracer for single- and double-labeling studies. J Neurosci Methods 1992; 41: 239–54.

Vivar C, Potter MC, Choi J, Lee JY, Stringer TP, Callaway EM, et al. Monosynaptic inputs to new neurons in the dentate gyrus. Nat Commun 2012; 3: 1107.

Waldau B, Shetty AK. Behavior of neural stem cells in the Alzheimer brain. Cell Mol Life Sci 2008; 65: 2372–84.

Weber K, Bartsch U, Stocking C, Fehse B. A multicolor panel of novel lentiviral "gene ontology" (LeGO) vectors for functional gene analysis. Mol Ther 2008; 16: 698–706.

Weber K, Thomaschewski M, Benten D, Fehse B. RGB marking with lentiviral vectors for multicolor clonal cell tracking. Nat Protoc 2012; 7: 839–49.

Weber K, Thomaschewski M, Warlich M, Volz T, Cornils K, Niebuhr B, et al. RGB marking facilitates multicolor clonal cell tracking. Nat Med 2011; 17: 504–9.

Williams A, Lucassen PJ, Ritchie D, Bruce M. PrP deposition, microglial activation, and neuronal apoptosis in murine scrapie. Exp Neurol 1997; 144: 433–8.

Winner B, Kohl Z, Gage FH. Neurodegenerative disease and adult neurogenesis. Eur J Neurosci 2011; 33: 1139–51.